CHAPTER 3
NONLINEAR RESONANCE ISLANDS AND ONE–DIMENSIONAL PERSISTENT SIGNALS

In this chapter a discrete Hamiltonian approach to two-dimensional transverse nonlinear resonances is presented that gives perturbative results exact to first order in nonlinear magnet strength. One-turn and N-turn Hamiltonians are derived from a projection map (Peggs 1982) in § 3.1-2 respectively; these Hamiltonians can be considered to respectively generate the one-turn and N-turn Poincaré surface of section maps. Certain phase space structures, called "resonance islands", can appear with one-dimensional resonant motion as pictured in Figure (3.1). These structures are shown to be parameterized by several experimentally accessible quantities including the island tune, $Q_{\rm I}$, in § 3.3; a computational single particle tracking simulation is described in § 3.4 and compared to theoretical prediction for the $5Q_x$ resonance. Various methods used to experimentally investigate nonlinear resonance islands are discussed in § 3.5, in particular those used in experiment CE22 at the IUCF Cooling Ring and for this thesis in experiment E778 at Fermilab.

3.1 THE FIRST ORDER NONLINEAR ONE–TURN HAMILTONIAN

In the previous chapter the action-angle parameterization was presented for the uncoupled linear transverse one-turn particle motion in a synchrotron. The next issue is how to include the effects of nonlinear magnets to form a discrete Hamiltonian that more adequately describes motion in a real accelerator. A perturbative approach that is correct to first order in nonlinear magnet strengths is used here; however, there exist a multitude of other methods, both perturbative (Michelotti 1986a) and non-perturbative (Gabella 1991), that give similarly-structured

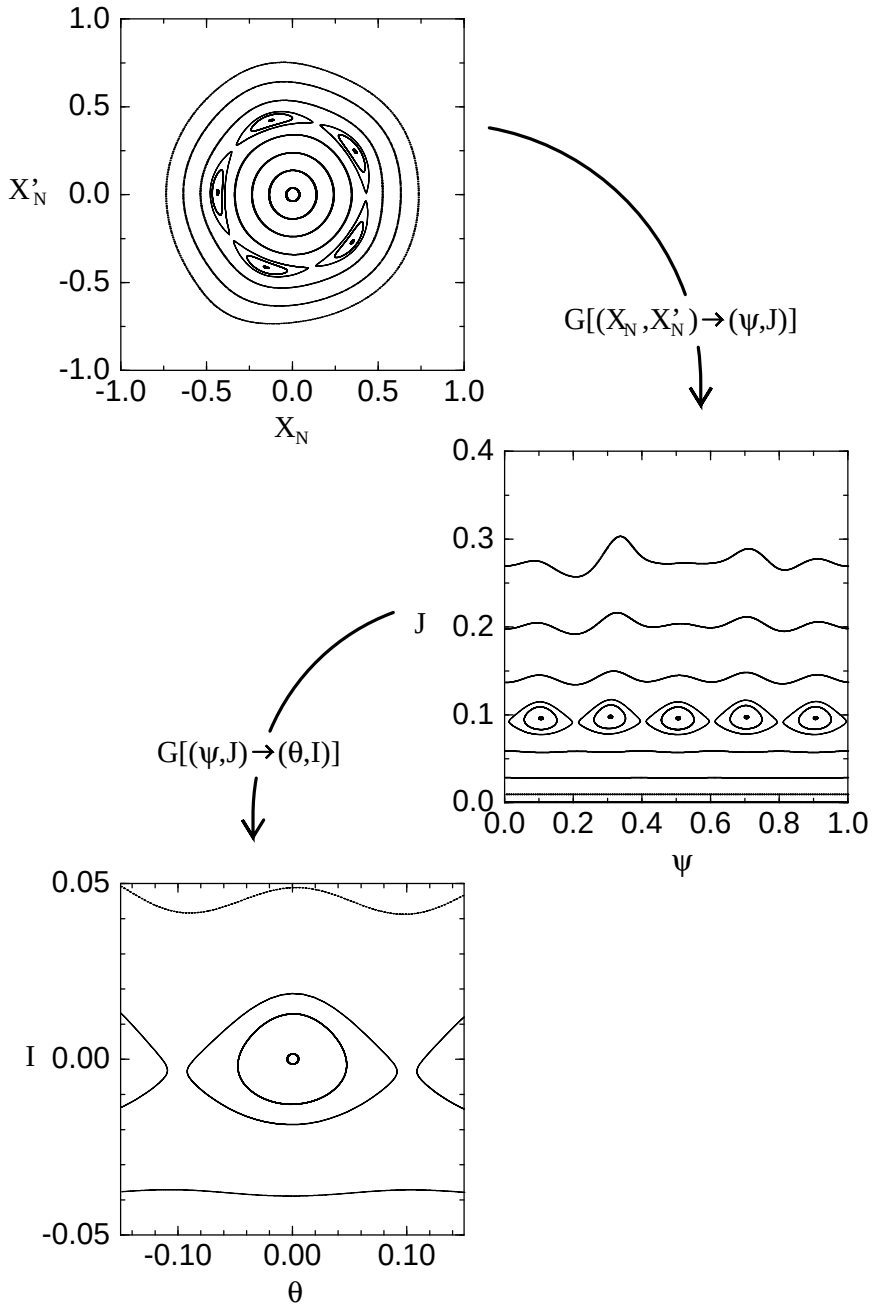

Figure 3.1: Isolated $5Q_x$ resonance islands in various phase space coordinate systems. Data is taken from simulation and tracking using the octupole/decapole lattice described in Section 3.4, which drives the resonance seen here to first order in decapole strength.

Hamiltonians.

Consider a synchrotron with a single thin nonlinearity of normalized strength $\tilde{b}_n$, where n represents the order of the nonlinearity. Transverse single-particle motion around the ring consists of three parts: a linear phase advance to the nonlinearity, the nonlinear kick and another linear phase advance back to the starting point. Since the linear portion of this motion is already well-described by the Hamiltonian of the previous chapter, it is removed here by a reverse rotation through the ring while ignoring the nonlinearity. This has the effect of projecting the kick at the phase advance of the nonlinearity to a nonlinear one-turn map of the initial particle coordinates.

Denote the horizontal and vertical phase advances at the location of the nonlinearity by $(\phi_{nl,x}, \phi_{nl,y})$ (as measured from a reference point) and the linear beta functions by $(\beta_{nl,x}, \beta_{nl,y})$. The nonlinear kicks at this location in normalized coordinates are then given by substitution the of normalized coordinate definitions into the nonlinear kick expansion, Equation (2.6):

$$\begin{aligned}
\Delta x'_N &= -\tilde{b}_n \sum_{k=0}^{n/2} \binom{n}{2k} (-1)^k \beta_{nl,x}^{\frac{n+1}{2}-k} \, x_N^{n-2k} \, \beta_{nl,y}^{k} \, y_N^{2k} \ , \\
\Delta y'_N &= \tilde{b}_n \sum_{k=0}^{n/2-1} \binom{n}{2k+1} (-1)^k \beta_{nl,x}^{\frac{n-1}{2}-k} \, x_N^{n-2k-1} \, \beta_{nl,y}^{k+1} \, y_N^{2k+1} \ .
\end{aligned} \tag{3.1}$$

This nonlinearity is a perturbation at a particular phase advance within the machine. To quantify this consider the "projection mapping":

$$\begin{pmatrix} \Delta x_N \\ \Delta x'_N \\ \Delta y_N \\ \Delta y'_N \end{pmatrix} = \mathbf{R}^{-1}(\phi_{nl,x}, \phi_{nl,y}) \begin{pmatrix} \mathbf{K}_x \\ \mathbf{K}_y \end{pmatrix} \mathbf{R}(\phi_{nl,x}, \phi_{nl,y}) \begin{pmatrix} x_N \\ x'_N \\ y_N \\ y'_N \end{pmatrix} \tag{3.2}$$

where $\mathbf{R}$ is the 4×4 block diagonal linear rotation matrix

$$\mathbf{R}(\phi_x, \phi_y) \equiv \begin{pmatrix} \cos\phi_x & \sin\phi_x & 0 & 0 \\ -\sin\phi_x & \cos\phi_x & 0 & 0 \\ 0 & 0 & \cos\phi_y & \sin\phi_y \\ 0 & 0 & -\sin\phi_y & \cos\phi_y \end{pmatrix} \tag{3.3}$$

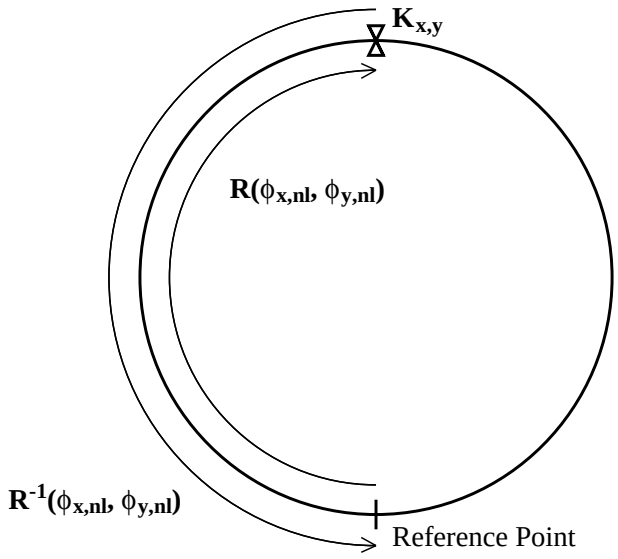

Figure 3.2: A simple lattice for the projection of a nonlinear kick onto a mapping of initial particle coordinates.

and the $\mathbf{K}_i$ symbolize the nonlinear kicks (3.1) in each plane. This accurately accounts for the nonlinear motion — the linear portion of the motion has been removed by the inverse rotation $\mathbf{R}^{-1}$.

If x'_N is the canonical momentum for x, the mapping of Equation (3.2) is actually integrable. A discrete one-turn nonlinear Hamiltonian $H_{1,nl}(x_N, x'_N, y_N, y'_N)$ can be written such that discrete forms of Hamilton's equations are obeyed as in the previous chapter:

$$\begin{pmatrix} \Delta x_N \\ \Delta x'_N \\ \Delta y_N \\ \Delta y'_N \end{pmatrix} = \begin{pmatrix} \partial H_{1,nl}/\partial x'_N \\ -\partial H_{1,nl}/\partial x_N \\ \partial H_{1,nl}/\partial y'_N \\ -\partial H_{1,nl}/\partial y_N \end{pmatrix} . \tag{3.4}$$

The Hamiltonian can be written in these coordinates but it is much more meaningful to write it in action-angle coordinates $(\psi_x, J_x, \psi_y, J_y)$, which are related to

the normalized coordinates via the canonical transformation

$$\begin{aligned} G_1([x_N, x'_N] \rightarrow [\psi, J]) &= -\frac{x_N^2}{2}\ \tan\psi \\ x_N &= \sqrt{2J}\cos\psi \\ x'_N &= -\sqrt{2J}\sin\psi \end{aligned} \tag{3.5}$$

in each plane. Including the linear portion of the motion and denoting the unperturbed linear base tunes by (Q_{x0}, Q_{y0}), we find the explicit form of the one-turn first-order nonlinear Hamiltonian:

$$\begin{aligned} H_1(\psi_x, J_x, \psi_y, J_y) &= 2\pi Q_{x0} J_x + 2\pi Q_{y0} J_y \\ &+\tilde{b}_n \sum_{k=0}^{n/2} \frac{n!\,(-1)^k\, 2^{\frac{n+1}{2}}}{(2k)!(n-2k+1)!} (\beta_{nl,x} J_x)^{\frac{n-2k+1}{2}} (\beta_{nl,y} J_y)^k \\ &\quad \times \cos^{n-2k+1}(\psi_x + \phi_{nl,x})\, \cos^{2k}(\psi_y + \phi_{nl,y})\ , \end{aligned} \tag{3.6}$$

where the $n/2$ limit in the sum is rounded up. This Hamiltonian may be written in another form as a useful ansatz:

$$\begin{aligned} H_1(\psi_x, J_x, \psi_y, J_y) =& 2\pi Q_{x0} J_x + 2\pi Q_{y0} J_y \\ &+ \frac{1}{2}\alpha_{xx} J_x^2 + \alpha_{xy} J_x J_y + \frac{1}{2}\alpha_{yy} J_y^2 \\ &+ \sum_{k,l} V_{kl}(J_x, J_y) \cos(k\psi_x + l\psi_y + \phi_{kl})\ . \end{aligned} \tag{3.7}$$

The first line of the Hamiltonian contains the linear phase advance terms as in the previous chapter. The second line contains some of the so-called "shear terms", which are not phase dependent but instead cause action-dependent tunes via

$$\begin{aligned} Q_x(J_x, J_y) &= \left\langle \frac{\partial H_1}{\partial J_x} \right\rangle = Q_{x0} + \frac{1}{2\pi}(\alpha_{xx} J_x + \alpha_{xy} J_y), \\ Q_y(J_x, J_y) &= \left\langle \frac{\partial H_1}{\partial J_y} \right\rangle = Q_{y0} + \frac{1}{2\pi}(\alpha_{xy} J_x + \alpha_{yy} J_y)\ . \end{aligned} \tag{3.8}$$

Here the brackets mean to average over all phases ϕ_x and ϕ_y — this phase averaging is explicitly incorrect in the case of resonant motion where only a certain subset of particle phases are reached.

The last line of the Hamiltonian (3.7) contains phase dependent terms, or resonances, that are driven by this multipole, obtained by expanding the trigonometric functions in Equation (3.6). Equation (3.7) is a general form of the Hamiltonian for all orders of the nonlinear strength, with first order terms given exactly by Equation (3.6); these are tabulated for sextupole, octupole and decapole magnets in Table (3.1). The V_{kl} coefficients are resonance strengths which depend on the actions, and the ϕ_{kl} are the relative phases of the resonance driving terms.

The treatment of several multipoles to first order is straightforward, because to that order there are no interactions between the nonlinearities. Thus the first-order nonlinear Hamiltonian for any collection of multipoles is simply the sum of their individual nonlinear Hamiltonians. For higher order nonlinear contributions to the α_{ij} and V_{kl} coefficients this procedure is inadequate, and other techniques must be used to evaluate these coefficients such as successive iteration of the discrete mapping (Peggs and Talman 1986), Deprit's algorithm (Michelotti 1986a,Michelotti 1986b) or application of successive Moser transformations (Merminga and Ng 1989).

Examination of Table (3.1) demonstrates that sextupoles contain no shear terms to first order, but instead drive three sets of nonlinear resonances: Q_x, $3Q_x$, and $Q_x \pm 2Q_y$. Shear terms quadratic in action, which correspond to detuning, are driven to second order in the sextupole strength; explicit formulae for this tune shift exist (Peggs and Talman 1986, Michelotti 1986a) and have been verified against simple particle tracking. Generally, the Hamiltonian of Equation (3.6) demonstrates that for a multipole kick of order n, the highest order resonance driven to first order in the multipole strength is $(n+1)Q = l$. For a head-on nonlinear beam-beam kick (see Equation (7.4)), in contrast, *all* even resonances are driven to first order in the small quantity parameterizing the kick.

The $5Q_x$ resonance investigated in E778 is explicitly directly driven to third

Hamiltonian Coefficient	**Lattice Value**
$V_{1,0}$	$\frac{\sqrt{2}}{4}\tilde{b}_2\ J_x^{1/2}\ [2J_x - J_y]$
$V_{3,0}$	$\frac{\sqrt{2}}{6}\tilde{b}_2\ J_x^{3/2}$
$V_{1,\pm 2}$	$-\frac{\sqrt{2}}{8}\tilde{b}_2\ J_x^{1/2} J_y$
α_{xx}	$\frac{3}{4}\ \tilde{b}_3$
α_{yy}	$\frac{3}{4}\ \tilde{b}_3$
α_{xy}	$-\frac{3}{2}\ \tilde{b}_3$
$V_{2,0}$	$\frac{1}{2}\ \tilde{b}_3\ J_x[J_x - 3J_y]$
$V_{0,2}$	$\frac{1}{2}\ \tilde{b}_3\ J_y[J_y - 3J_x]$
$V_{2,\pm 2}$	$-\frac{3}{4}\ \tilde{b}_3 J_x J_y$
$V_{4,0}$	$\frac{1}{8}\ \tilde{b}_3 J_x^2$
$V_{0,4}$	$\frac{1}{8}\ \tilde{b}_3 J_y^2$
$V_{5,0}$	$\frac{\sqrt{2}}{20}\ \tilde{b}_4 J_x^{5/2}$
$V_{3,0}$	$\frac{\sqrt{2}}{4}\ \tilde{b}_4 J_x^{3/2}\ [J_x - 4J_y]$
$V_{1,0}$	$\frac{\sqrt{2}}{2}\ \tilde{b}_4 J_x^{1/2}\ \left[J_x^2 - 6J_x J_y + 3J_y^2\right]$
$V_{1,\pm 2}$	$\frac{\sqrt{2}}{2}\ \tilde{b}_4 J_x^{1/2} J_y\ [2J_y - 3J_x]$
$V_{3,\pm 2}$	$-\frac{\sqrt{2}}{2}\ \tilde{b}_4 J_x^{3/2} J_y$
$V_{1,\pm 4}$	$\frac{\sqrt{2}}{4}\ \tilde{b}_4 J_x^{1/2} J_y^2$

Table 3.1: First-order Hamiltonian coefficients in Equation (3.7) for sextupole, octupole and decapole magnets. The beta functions scale into these with the actions $J_{x,y}$, but have been set equal to one here for clarity. For the octupole-decapole lattice octupole detuning coefficients α_{ij} are tripled due to the presence of three octupoles.

order in sextupole strength (Merminga and Ng 1992,Michelotti 1986b). However, it has been hypothesized that the structure of this resonance may be adequately reproduced at a lower order by interference between the $3Q_x$ and $2Q_x$ resonances (Michelotti 1991). This issue remains a subject of debate; in either event the resonance strength driving by sextupoles is smaller than the first-order approach presented here.

3.2 THE ONE–DIMENSIONAL NONLINEAR N–TURN HAMILTONIAN

The general multi-resonance Hamiltonian as given in Equation (3.7) is extremely difficult to investigate analytically. Instead we examine an explicitly one-dimensional case ($J_y = 0$), dropping the (x, y) subscripts. We also assume that the horizontal base tune Q_0 is very close to a one-dimensional resonance: $Q_0 \equiv M/N + \delta_Q$, where $\delta_Q \ll 1/N$. Under these conditions, we shall show that the Hamiltonian is approximately that of a isolated resonance model with a family of elliptically stable N-turn fixed points and that motion around any of these stable fixed points can be transformed to a form approximating that of a classical free pendulum (Chirikov 1979).

One difficulty of the discrete Hamiltonian is the discontinuous nature of the phase advance — if the tune is not near an integer the net phase advance every turn is large. However, with the assumption that the tune is near the resonance M/N, the accumulated phase advance over N turns is very close to $2\pi M$ and thus effectively small. It therefore makes sense to look at a difference Hamiltonian that reproduces a Poincaré surface of section not every turn, but every N turns. Alternatively, one could embed this system in a system of higher dimensionality (Vivaldi 1984), but the method of integrating (summing) the Hamiltonian explicitly at low orders is more intuitive for this application.

When examining N-turn motion, the time variable needs to be changed from

$t = 0, 1, \ldots$ to "N-turns", $T \equiv t/N = 0, 1, \ldots$, as stated in the previous chapter. One must also be careful to distinguish the relevant timescales for frequency-domain variables; from here on any frequency variable, say Q, is defined to be the frequency of oscillations in the one-turn timescale:

$$\sin(2\pi Q t) = \sin(2\pi Q N T) \; . \tag{3.9}$$

Dropping x and y subscripts and setting $J_y = 0$, the general one-turn one-dimensional Hamiltonian can be written from Equations (3.6) and (3.7) as

$$H_1(\psi, J) = 2\pi Q_0 J + \frac{1}{2}\alpha J^2 + \sum_{k,k'} V_{kk'} J^{k/2} \cos(k'\psi + \phi_{kk'}) \; . \tag{3.10}$$

It is important to note that the action dependence has been removed from the resonance strength $V_{kk'}$ here and inserted as a sum of its own. Summing this Hamiltonian over N turns and approximating the action J as constant over these N turns gives

$$\begin{aligned} H_N(\psi, J) = & 2\pi N \delta_Q J + \frac{N}{2}\alpha J^2 \\ & + \sum_{k,k'} V_{kk'} J^{k/2} \sum_{i=0}^{N-1} \cos\left[k' \left(\psi + \frac{2\pi i M}{N} + 2\pi i \delta_Q \right) + \phi_{kk'} \right] \; . \end{aligned} \tag{3.11}$$

Only the linear contribution to the phase advance has been included in the resonance terms since this analysis is to first order in the nonlinear terms $V_{kk'}$ and α. The sum over i in (3.11) is easily found by using the identity

$$\begin{aligned} \sum_{i=0}^{N-1} \cos(A + iB) &= \mathcal{D}(B, N) \cos(A + \frac{N-1}{2} B) \; , \\ \mathcal{D}(B, N) &\equiv \frac{\sin(NB/2)}{\sin(B/2)} \; . \end{aligned} \tag{3.12}$$

$\mathcal{D}(B, N)$ is extremely similar to the Dirichlet kernel found in the theory of Fourier series; it is very strongly peaked at values of B where the difference between B/π and the nearest integer is much less than $1/N$, in which case its value is

approximately N. In this case $B/\pi = 2k'(M/N + \delta_Q)$, and so the only terms that contribute significantly are terms where k' is a multiple of N. (This is in practice an approximation, because very large resonance strengths, possibly from lower order terms, can overcome this suppression.) For typical multipole magnets encountered in accelerators (i.e. small order, n) the $k' = N$ term will dominate, and there will be only one resonant term that contributes. In this case we have the isolated resonance N-turn Hamiltonian

$$\begin{aligned} H_N(\psi, J) = & 2\pi N \delta_Q J + \frac{N}{2}\alpha J^2 \\ & + N V_N J^{N/2} \cos[N\psi + \phi_N] \\ & + \text{suppressed resonance terms} , \end{aligned} \tag{3.13}$$

where a constant phase offset $N(N-1)\pi\delta_Q$ has been absorbed into ϕ_N.

3.3 PARAMETERIZATION AND CHARACTER OF RESONANT MOTION

Now that we have this Hamiltonian, we can answer the question of how the small nonlinearity distorts the normal linear phase space motion of particles within an accelerator. With no resonance driving at all (i.e. only linear and shear terms) particles still trace out circular trajectories in (x_N, x'_N) space, with radii $\sqrt{2J}$ and phases ψ. However, the particle tunes are action-dependent due to the shear terms in the Hamiltonian. This section will show that when a resonance term is introduced with shear terms present, structures called "resonance islands" are formed in phase space that can be parameterized in a way completely equivalent to free pendulum motion.

Applying the discrete forms of Hamilton's equations to the N-turn Hamiltonian of Equation (3.13) gives, over N turns,

$$\Delta\psi = \frac{\partial H_N}{\partial J} = 2\pi N \delta_Q + N\alpha J + \frac{N^2}{2} V_N J^{N-2/2} \cos(N\psi) \tag{3.14}$$

and

$$\Delta J = -\frac{\partial H_N}{\partial \psi} = N^2 V_N J^{N/2} \sin(N\psi) \ . \tag{3.15}$$

The map described by Equations (3.14) and (3.15) exhibits N-turn fixed points when both ΔJ and $\Delta\psi$ are zero. The constraint $\Delta J = 0$ gives one trivial solution ($J_{fp} = 0$) and $2N$ fixed points at the phases $\psi_{fp} = k_{res}\pi/N$, where k_{res} is an integer. Using these phases in Equation (3.14) then gives the equation for J_{fp}:

$$2\pi\delta_Q + \alpha J_{fp} \pm \frac{N}{2} V_N J_{fp}^{\frac{N-2}{2}} = 0 \tag{3.16}$$

where the top sign refers to even k_{res}, and the bottom to odd k_{res}. This equation for the fixed-point action is in general transcendental, but can be exactly solved for all N below 7. Note that when no positive real solutions exist for J_{fp}, there are no fixed points. In practice the detuning term is usually much larger than the resonance term, in which case an approximate solution is $J_{fp} \approx -2\pi\delta_Q/\alpha$.

We can now apply a last linear transformation to the Hamiltonian, by expanding the N-turn Hamiltonian (3.13) around these fixed points with the linear (canonical) translation

$$\begin{aligned} \psi &= \psi_{fp} + \theta \ , \\ J &= J_{fp} + I \ . \end{aligned} \tag{3.17}$$

The expansion action I is assumed to be small with respect to the magnitudes of the fixed points action, so $I \ll J_{fp}$; no such constraint is placed on θ. The final Hamiltonian is then found to be

$$H_N(\theta, I) = \frac{N}{2}\alpha I^2 \pm N V_N J_{fp}^{N/2} \cos(N\theta) + \mathcal{O}(V_N I) \ . \tag{3.18}$$

If αV_N is negative, there is a family of N elliptic (stable) fixed points (at phases $\theta = 0, 2\pi/N, \ldots$, corresponding to even k_{res}), surrounded by a separatrix intersecting another family of N hyperbolic fixed points (at phases $\theta = \pi/N, 3\pi/N, \ldots$, corresponding to odd k_{res}); if αV_N is positive the converse is true. We assume the

latter and choose the negative sign in this Hamiltonian to examine local motion around a stable fixed point.

Motion within the separatrix is termed "resonant" or "phase-locked" — particles within this region have a long-term average phase advance per turn, or tune, of *exactly* M/N. Particle trajectories just outside of the separatrix are distorted but nonresonant, as seen in Figure (3.1). Consider a set of particles populating one of these resonance islands at one particular time in the accelerator; this ensemble of particles will advance from island to island turn by turn in a completely coherent fashion. A position measurement of the centroid of this distribution will exhibit a coherent oscillation. This oscillation can in practice be observed on a online spectrum analyzer as a "persistent signal" at exactly the resonant tune, and with unperturbed resonance islands it typically has an exceptionally long lifetime of millions of turns.

Ignoring terms of order $V_N I$ and higher, Equation (3.18) is a free pendulum Hamiltonian and the equation of motion for θ that arises is

$$\begin{aligned} \ddot{\theta} &= -N^3 \alpha V_N J_{fp}^{N/2} \sin(N\theta) \\ &= -N(2\pi Q_{\mathrm{I}})^2 \sin(N\theta) \ , \end{aligned} \tag{3.19}$$

where the time derivatives are taken with respect to the "N-turn" time variable T, and Q_{I} (the "island tune", or frequency of small librations of this pendulum system) is defined by

$$Q_{\mathrm{I}} \equiv \frac{1}{2\pi} N J_{fp}^{N/4} \sqrt{|\alpha V_N|} \ . \tag{3.20}$$

A typical island tune observed in the E778 experiment is approximately 0.006, with similar values given by tracking with realistic nonlinear magnet strengths.

The island half-width δI can also be found from the Hamiltonian, because this Hamiltonian is autonomous. The separatrix is a contour along which the Hamiltonian is constant, and so the Hamiltonian value at an unstable fixed point

is equal to the Hamiltonian value at a stable fixed point phase with actions $\pm\delta I$:

$$H_N(\theta = \pi/N, I = 0) = H_N(\theta = 0, I = \pm\delta I) \rightarrow$$
$$\delta I = 2J_{fp}^{N/4}\sqrt{\left|\frac{V_N}{\alpha}\right|}\,. \tag{3.21}$$

Knowledge of the base tune Q_{x0} (and thus δ_Q), the island tune $Q_{\rm I}$ and the detuning α allows deduction of the fixed point action J_{fp}, island size δI and resonance driving strength V_N.

Since the motion is that of a pendulum within the resonance island, particles at different actions within the island circulate with different frequencies or tunes. These tunes range from the island tune $Q_{\rm I}$ at actions near zero to zero frequency on the separatrix, and can be written in terms of elliptic integrals. This nonlinear dependence of frequency with action (or amplitude) of the pendulum system makes measurement of $Q_{\rm I}$ more difficult, for only particles with actions near the fixed point action actually rotate in the island with this tune.

3.4 FIRST ORDER NONLINEAR TRACKING AND SIMULATION

For the issues investigated in this thesis, it was deemed necessary to design a dedicated simulation program that tracked a minimal lattice which drives relevant terms in the nonlinear Hamiltonian to first order. The Octupole-Decapole model lattice is designed with this goal in mind; it also uses sets of specially placed quadrupoles to independently control tune modulation and beta modulation at the resonance-driving nonlinearity. For simplicity, all beta functions are set at one meter in the following discussion and within the tracking codes themselves.

The lowest order multipoles that drive action-dependent nonlinear detuning of the form αJ^2 are octupoles, as seen in Table (3.1). To first order all resonance terms contributed by the octupoles should vanish in the simulation. This enables complete separation between detuning, the function of the octupoles, and resonance driving from the decapole. It is possible to eliminate all but one of the first

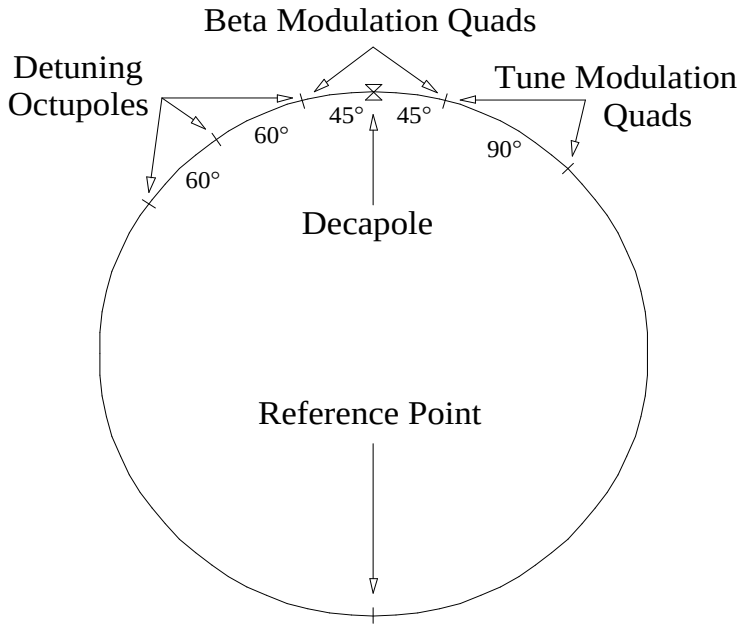

Figure 3.3: The octupole-decapole lattice.

order octupole resonances, the diagonal coupling resonance $2Q_x - 2Q_y$, by driving three octupoles with the same strength, spaced apart by a betatron phase advance of $60° = 2\pi/3$ between each octupole. This also triples the phase-independent detuning coefficients α_{ij} over their single octupole values. The decapole is used to drive the $5Q_x$ resonance, motivated by the study of this resonance in E778.

To investigate the effects of tune modulation and beta modulation, the linear phase advances in the lattice were set to constant values and only special quadrupoles explicitly introduced into the lattice were modulated. Three quadrupoles are sufficient to independently control the tune modulation of the lattice and beta modulation at the resonance-driving decapole. The tune shift from a single small quadrupole error is given by Equation (2.22), recalling $\beta_x = \beta_y = 1m$ for this lattice,

$$\Delta Q(\text{quad}) = \frac{\tilde{b}_1}{4\pi} \, . \tag{3.22}$$

This is independent of the phase of the quadrupole within the machine, so a pair of modulated quadrupoles driven with the same sign will produce tune modulation with strength $q = 2\Delta Q = \tilde{b}_1/2\pi$. The beta modulation created by a quadrupole error is given by Equation (4.4),

$$\Delta\beta(s) = \frac{\tilde{b}_1}{2}\left[\sin(2|\phi(s) - \phi_{quad}|) - \cos(2|\phi(s) - \phi_{quad}|)\tan(2\pi Q_0)\right] \ . \qquad (3.23)$$

Two quadrupoles driven with equal strength, opposite sign and 90° apart in phase advance will destructively interfere outside of this phase advance. They constructively interfere within the 90° phase advance, and at a point exactly halfway in between them they will modulate the beta function with strength $b = \Delta\beta = \tilde{b}_1$, with no tune modulation since the quadrupoles are driven with equal and opposite strengths.

The elements of this lattice are shown in Figure (3.3); the phase advances outside the cluster of quadrupoles and nonlinear elements are set by the two constraints that the linear tunes are some set values, say (Q_{x0}, Q_{y0}), and the decapole is positioned exactly halfway through the lattice from the reference point, so $\phi_{dec} = \pi Q_0$ in each plane.

A one-dimensional tracking program, OdTrack, has been written which tracks single particles through horizontal phase space in this lattice and includes the effects of either or both tune modulation and beta modulation. The inputs to this program include the horizontal base tune, the octupole and decapole strengths $\tilde{b}_3$ and $\tilde{b}_4$, the amplitude and period (in turns) of the modulation and the number of turns to track. Particles can be launched at a variety of amplitudes but only at a single phase during every execution of the simulation. Output includes the phase space coordinates of every particle for each synchrotron period and the measured tune of each particle over the entire tracking run.

Timing tests on a Sparcstation IPX show an iteration CPU time of 33 μs per

turn, making million-turn tracking with this lattice easily accessible. Raising the timescales by several orders of magnitude to examine thousands of millions of turns (or millions of synchrotron periods) of evolution still only requires tens of hours of processing time, and is quite feasible.

The prediction for the island tune of Equation (3.20) is proportional to the square root of both the detuning α and the resonance driving strength V_5. However, with the approximation that $V_5 J_{fp}^{\frac{-1}{2}} \ll \alpha$ in Equation (3.16) for the fixed point action J_{fp}, it is apparent that the fixed point action also varies inversely with the detuning. Therefore, since the resonance strength V_N is driven to first order in the decapole strength and the detuning is driven to first order in octupole strength (see Table [3.1]), the island tune is expected to vary as:

$$Q_{\mathrm{I}} \propto \tilde{b}_3^{\frac{-3}{4}} \; \tilde{b}_4^{\frac{1}{2}} \; . \tag{3.24}$$

Figure (3.4) shows a comparison of the theoretical prediction for Q_{I} to tracking in this lattice while varying the octupole strength, showing the scaling of (3.24) for small $\tilde{b}_3$. As this strength becomes nonperturbatively large (on the order of $3\tilde{b}_3 \approx 1$, since there are three octupoles in this lattice), the naive first order predictions fail. This is due to a higher-order contribution to the resonance driving by the octupoles which cannot be ignored in this limit. However, for octupole strengths smaller than .1 $\mathrm{m}^{-3/2}$, the results of first order perturbation theory appears adequate.

Figure (3.5) shows a similar comparison while varying the decapole strength, keeping the octupole strengths constant. Here the approximation begins to fail at lower orders as the $3Q_x$ resonance, also driven to first order in $\tilde{b}_4$, begins to distort the phase space where the resonance islands are located. For decapole strengths less than 10^{-3} m^{-2}, at the octupole strength listed, the prediction and scaling of (3.24) agree with tracking.

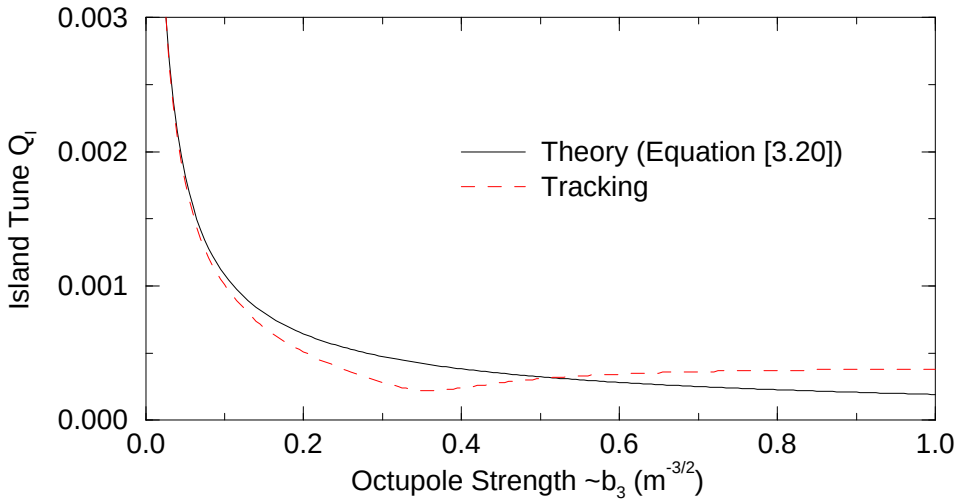

Figure 3.4: A comparison of the theoretical prediction for the island tune Q_{I} to tracking in the octupole-decapole lattice, varying the octupole strength $\tilde{b}_3$. This comparison is for the $5Q_x$ resonance ($Q_0 = 2/5$) with $\delta_Q = -0.02$, and the decapole strength is constant at $\tilde{b}_4 = 5 \cdot 10^{-4}\ \mathrm{m}^{-2}$.

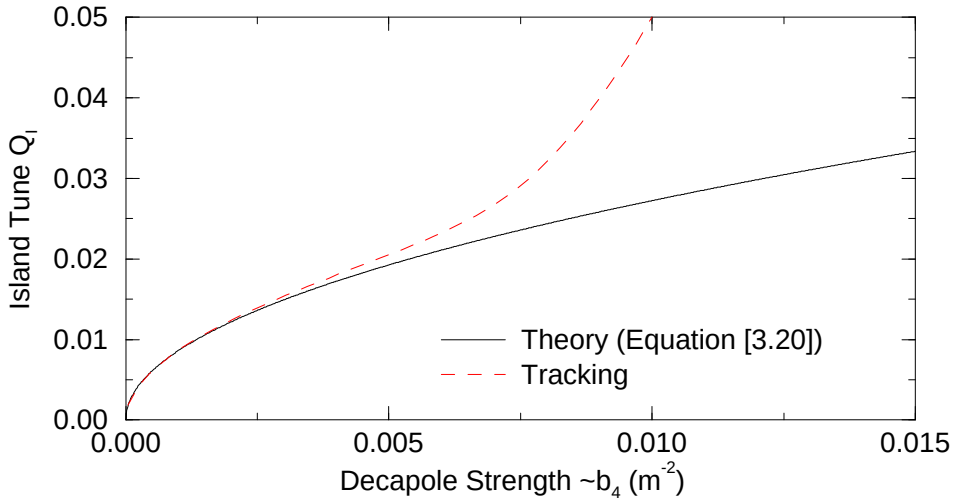

Figure 3.5: A similar comparison as the above figure, now keeping the octupole strength constant at $\tilde{b}_3 = 10^{-2}\ \mathrm{m}^{-3/2}$ and varying the decapole strength $\tilde{b}_4$.

3.5 MEASUREMENTS IN REAL ACCELERATORS

The detuning coefficient α can be experimentally measured in several ways. One method is to kick the beam transversely and observe the resulting tune shift at this betatron amplitude. This is typically only possible if the beam is small enough such that there is no appreciable tune spread over the beam distribution, due to the presence of tune spread decoherence as discussed in the next paragraph. This is also the method used by tracking programs to measure the tune dependence on amplitude, because the phase advance for a single particle can be measured to the computational precision and there is no tune spread or decoherence in single-particle motion.

With a moderately sized beam, the detuning coefficient can be measured by observing the decoherence time of a bunch kicked into a non-resonant section of phase space. Particles that comprise a kicked bunch will have different tunes (because of their different amplitudes after the kick), and so the distribution will "decohere", with the phases of particles with smaller tunes lagging further and further behind those of particles with larger tunes. The timescale for this phenomena to decohere the beam is

$$\tau(\text{decohere}) = \frac{1}{\left(\frac{dQ}{dJ}\right)_{J(\text{kick})} \cdot \sigma} , \tag{3.25}$$

where $J(\text{kick})$ is the action of the kick and σ is the size of the beam measured in units of the action. For conditions experienced in experiment E778, the typical decoherence time is tens to hundreds of machine turns. This phenomenon has been previously studied, both within the context of E778 (Chao et. al. 1987b, Chao et. al. 1988, Merminga 1989) and in other environments (Lee et. al. 1991, Byrd 1992). It gives a quantitative measurement of the detuning strength even when the coherent oscillation decays rapidly and direct measurement of the tune at the new

betatron amplitude is impossible. An illustration of this decoherence is shown in Figure (3.6), and an actual experimental turn-by-turn position measurement showing this decoherence is shown in Figure (3.9).

With this independent measure of α, one now needs to know the island tune or island width in order to deduce the resonance strength. The island width has been measured in past E778 experimental runs by observing the fraction of kicked beam trapped within a resonance island (Chao et. al. 1988, Merminga 1989). A typical value of the physical island width, $\sqrt{\delta I \beta_x}$, reported by Merminga is half a millimeter. This method usually can only give general estimates of δI, and relies on fine calibration of the kicker.

Instead, recent experiments have concentrated on measuring $Q_{\rm I}$, the island tune, in machines where strong resonances have been driven by explicitly introduced nonlinearities. Sextupoles have predominantly been used, since they are the lowest order nonlinear multipoles and are commonly found in many accelerators to correct chromatic focusing errors. The procedure of finding and populating such resonance islands in the phase space of a real machine is greatly simplified by the appearance of "persistent signals" when a significant fraction of the beam is captured within a resonance island. When this occurs, the trapped beam exhibits a coherent oscillation with an exceptionally long lifetime — millions of turns — and the frequency spectrum of the beam on an online spectrum analyzer shows a long-lived peak exactly at the resonant frequency.

One possible method to determine the island tune is to examine the coherent motion of a bunch kicked into a resonance island. If the bunch is small enough (ie. has an RMS size much smaller than the size of the island), it behaves essentially as a single particle for times much smaller than it's decoherence time within the island. The resulting coherent motion within the resonance allows direct measurement of $Q_{\rm I}$; such an approach was adopted by the CE22 collaboration at

IUCF (Lee et. al. 1991). Figure (3.7) shows a representation of such a kick applied to the resonant system seen in Figure (3.6).

In the Fermilab Tevatron, beam sizes are typically large compared to the size of induced resonance islands; creation of larger resonance islands is impractical due to physical aperture considerations. This means that when the beam is kicked onto the resonance, the entire resonance island is populated. There is still a strong persistent signal corresponding to the coherent motion from island to island, but there is no local coherent motion of the particles trapped within the resonance island that allows direct observation of Q_{I}. Figure (3.8) shows a symbolic representation of such a kick, including the decoherence of the portion of the beam not trapped within the resonance island. A sample turn-by-turn position measurement from E778 showing this decoherence and a persistent signal is seen in Figure (3.10), showing beam capture on a $5Q_x$ resonance island chain.

There are various frequency-domain methods of examining the distribution of particles filling a single resonance island (Chen 1990). For example, if the resonance island is completely but not evenly populated, the discrete Fourier transform of a BPM measurement taken every N turns should show a low-frequency element similar to that of an ensemble of driven pendula, dropping off quickly into background noise at frequencies near the island tune.

Since the distribution of particles within the resonance island was indeed expected to be relatively even due to the nature of the beam size used in E778, another method is investigated in this thesis. Resonantly captured beam was excited with a set of very weakly modulated quadrupoles, modulating the tune and effectively turning the ensemble of free pendula into driven pendula. The frequency response of the beam was then correlated to the frequency of the modulation for a reasonable measurement of the island tune.

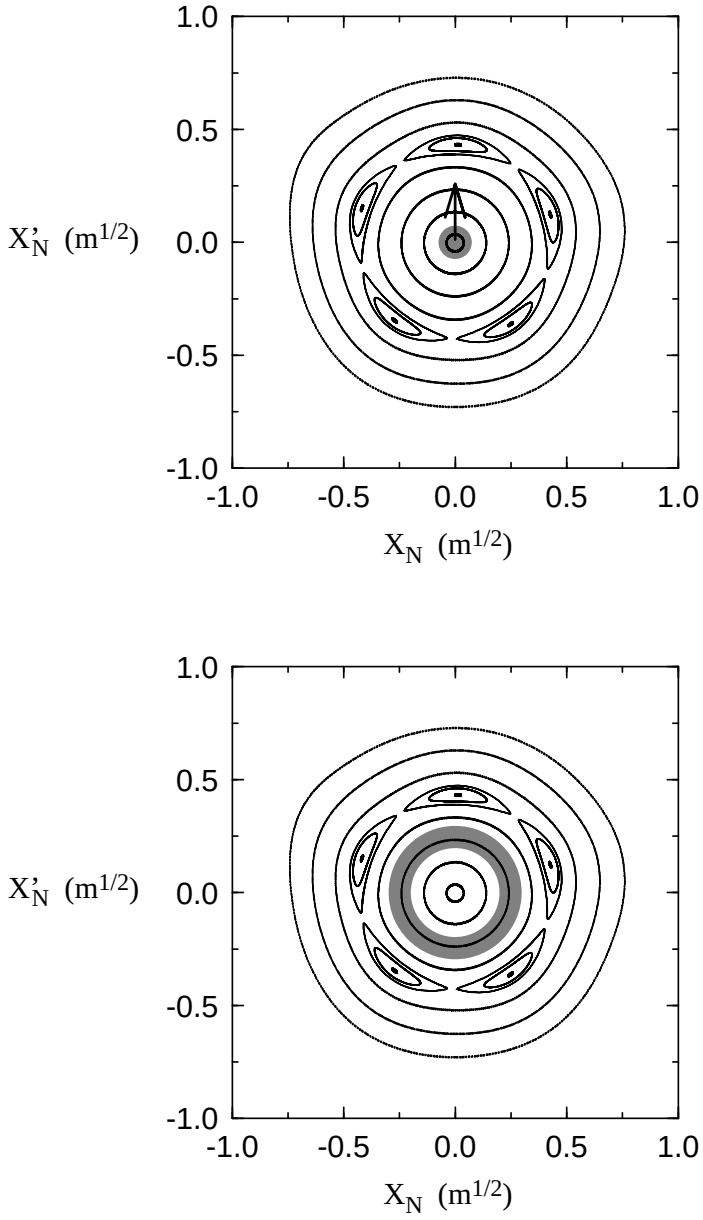

Figure 3.6: Beam decoherence from a kick into a sheared non-resonant section of phase space. The intermediate distribution has a centroid position that decays with time and approaches a final annular distribution (which has a larger emittance than the initial distribution and a centroid position of zero) over approximately hundreds of turns.

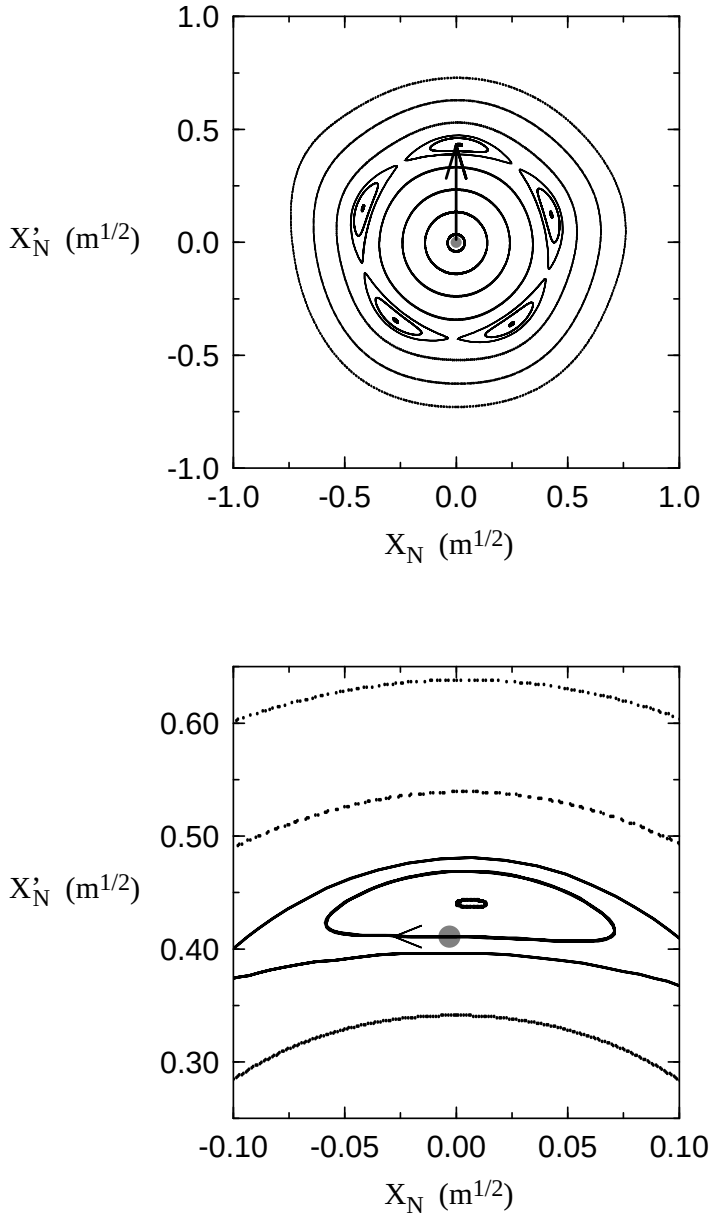

Figure 3.7: Phase space plot of a small beam kicked into an $N = 5$ nonlinear resonance island. Measurement of the centroid of the kicked distribution every 5 machine turns shows coherent motion around the center of the island, making direct measurement of the island tune Q_{I} possible.

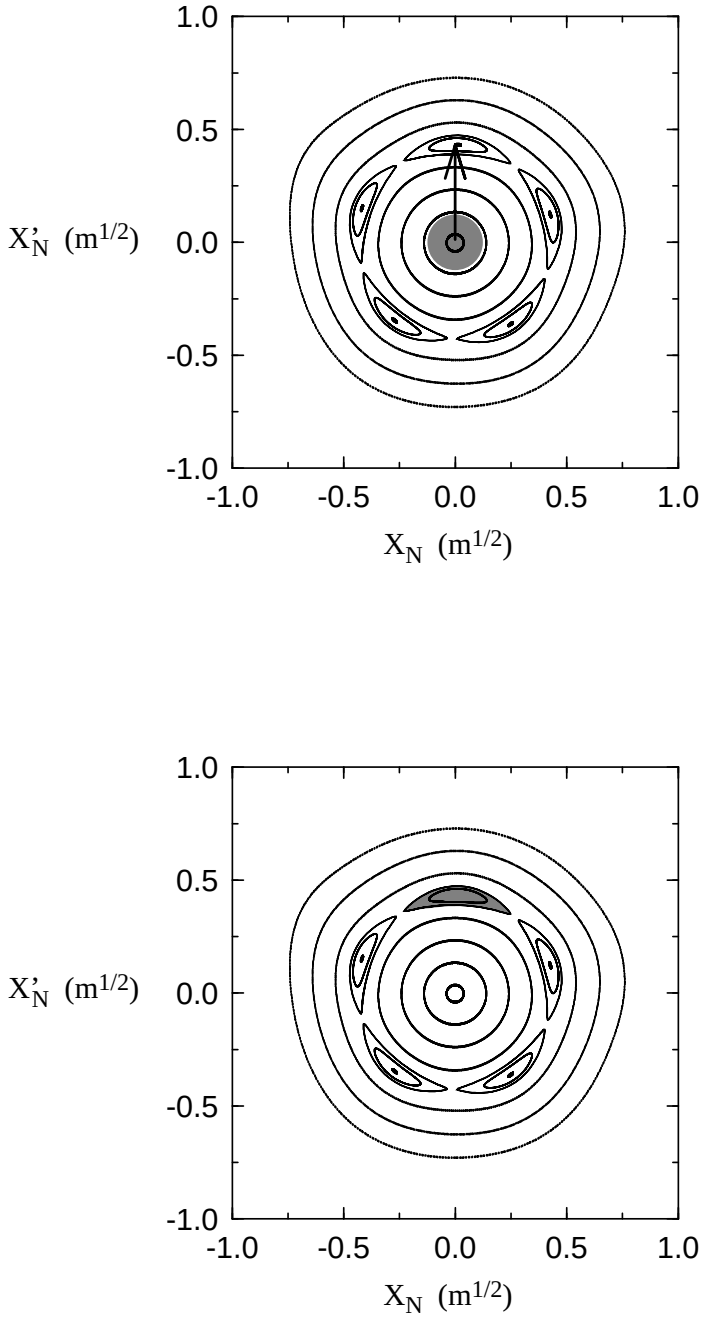

Figure 3.8: Phase space plot of a large beam kicked into an $N = 5$ nonlinear resonance island. The untrapped portion of the beam decoheres and does not contribute to the coherent centroid motion. The trapped portion coherently moves between resonance islands, but shows no evidence of the island tune Q_{I}.

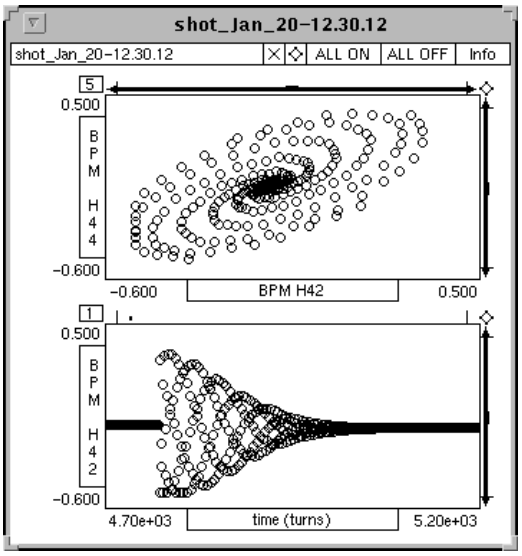

Figure 3.9: Sample E778 turn-by-turn data at kick time, showing the kick and gaussian decoherence. Kicker voltage is 11 kV, in the E778 91_0 lattice. The graphics are produced by the kaspar graphics program. The decoherence pictured has a timescale of approximately 100 turns.

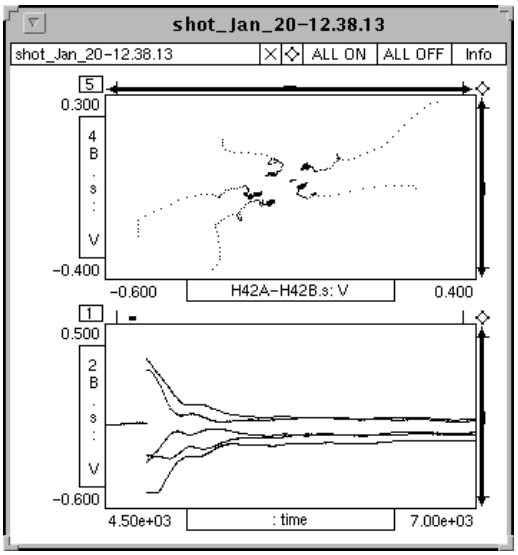

Figure 3.10: Sample turn-by-turn data at kick time for two BPMs separated by a betatron phase of approximately 70 degrees, showing the kick and production of a $Q_x = 20.40$ persistent signal. Kicker voltage and lattice are as in above figure. Only 2500 turns are pictured here, but this coherent oscillation survives for millions of turns.